

# Human Motion Segmentation using Cost Weights Recovered from Inverse Optimal Control

Jonathan Feng-Shun Lin, Vincent Bonnet, Adina M. Panchea,  
Nacim Ramdani, Gentiane Venture, and Dana Kulić

**Abstract**—A common hypothesis in human motor control is that human movement is generated by optimizing with respect to a certain criterion and is task dependent. In this paper, a method to segment human movement by detecting changes to the optimization criterion being used via inverse optimal control is proposed. The control strategy employed by the motor system is hypothesized to be a weighted sum of basis cost functions, with the basis weights changing with changes to the motion objective(s). Continuous time series data of movement is processed using a sliding fixed width window, estimating the basis weights of each cost function for each window by minimizing the Karush-Kuhn-Tucker optimality conditions. The quality of the cost function recovery is verified by evaluating the residual. The successfully estimated basis weights are averaged together to create a set of time varying basis weights that describe the changing control strategy of the motion and can be used to segment the movement with simple thresholds. The proposed algorithm is first demonstrated on simulation data and then demonstrated on a dataset of human subjects performing a series of squatting tasks. The proposed approach reliably identifies the squatting movements, achieving a segmentation accuracy of 84%.

## I. INTRODUCTION

The central nervous system, as the controller of the body, can choose from an unlimited number of joint trajectories in order to carry out an action. However, literature in human motor control over the last three decades has shown that the joint trajectory variance is limited to a much smaller subset, likely a minimization of a cost function [1]. Studies in biomechanics and human motion analysis have proposed many possible cost functions, such as minimizing time, joint velocity, or acceleration [2]. Given a human motion trajectory and a set of cost function hypotheses, the cost function used to generate the motion can be estimated via the use of *inverse optimal control* (IOC) [3]. Previous studies [4] show that different cost functions are used for different movements. Existing works typically segment continuous movement into discrete motion primitives and assume that the cost function does not change over the duration of a single primitive.

However, a continuous movement sequence may consist of multiple motion primitives, and each primitive may not necessarily share a common control strategy. This paper proposes that if the control strategy can be estimated as a function of the motion data, then a change in strategy may

be used as an indication that the motion primitive being performed has changed, and be used to segment the motion. To achieve this, a sliding window over the trajectory data is used to determine the basis weights of the cost function using IOC. The basis weights are averaged together to form a time varying feature of the motion trajectory. A threshold can be applied to this feature to perform motion segmentation.

Motion segmentation is the process of extracting motions of interest from continuous observation of motion data [5]. It has numerous applications, including imitation learning [6], human-robot interaction [7], rehabilitation [8], and activity recognition [9]. Existing approaches for human motion segmentation have primarily relied on kinematic data, such as joint angles [10], [11], Cartesian data [12], [13], and inertial measurement data [14], [15]. It is difficult to generalize from one participant to another using these features as they are dependent on participant stature, fitness, and data collection methods, and require substantial normalization and post-processing. This is especially a problem in health and rehabilitation applications, where methods developed using data collected from healthy participants typically do not generalize to injured or rehabilitating participants [5].

The use of IOC for human motion analysis has recently received increasing attention in biomechanics and robotics [16], [17], [18]. Previous work typically formulates the cost function being optimized by the central nervous system as a weighted sum of basis cost functions, so that the IOC problem can be solved by finding the basis function weights. Two primary methods have been proposed to solve the resultant optimization. The first is the *bi-level optimization* approach, where the basis weights are found by minimizing the root-mean-square error (RMSE) between the optimal path generated from the estimated weights and the observed data. Two layers of optimization are employed; one to generate the optimal trajectory given the weights and the task constraints, and the other to generate weights that minimize the RMSE given the trajectory. This method has been used in locomotion [3], [19], [17], reaching [20], [21], and overhead assembly [22] tasks. The bi-level optimization approach is flexible as it does not require the optimization gradient in analytical form, but is computationally demanding as it must both optimize the weights and minimize the RMSE [22].

The other technique formulates the IOC problem using the *inverse Karush-Kuhn-Tucker (KKT)* [23] optimality criteria, which is a set of criteria that are satisfied at the optimal solution. This transforms the initial optimization problem, which can be a constrained non-linear problem, into an

J. Lin and D. Kulić are with the University of Waterloo, Waterloo, Canada (email: {jf2lin, dkulic}@uwaterloo.ca). V. Bonnet and G. Venture are with the Tokyo University of Agriculture and Technology, Tokyo, Japan (email: bonnet.vincent@gmail.com, venture@cc.tuat.ac.jp). A. Panchea and N. Ramdani are with the Université d'Orléans, Bourges, France (email: nacim.ramdani@univ-orleans.fr, adina.panchea@gmail.com).

unconstrained problem. This method has found application in locomotion [24], [25], [16], [18] and box moving [26] tasks. KKT-based methods are faster than the bi-level optimization methods as they are only solving for the basis weights and the reconstructed trajectory is only calculated once to quantify the RMSE. However, the gradient must be modelled explicitly, which is not trivial [26].

This paper hypothesizes that the human motion control objective can be represented as a weighted sum of basis functions and applies IOC to a sliding window over observation data to recover the weights of the windowed trajectory. The weight vector at a given timestep is calculated as the average of all the windows that include that timestep and also have sufficiently low KKT error residual. Motion segmentation is performed on the recovered weights to segment the continuous time series trajectory into discrete actions.

## II. PROPOSED APPROACH

In this paper, the cost function  $J(\mathbf{x})$  that is minimized to generate a given motion is modelled as a weighted sum of basis cost functions  $J_{bf,i}(\mathbf{x})$ :

$$J(\mathbf{x}) = \sum_{i=0}^{n_{bf}} c_i J_{bf,i}(\mathbf{x}) \quad (1)$$

where  $\mathbf{x}$  is the variable that is manipulated to minimize the cost. The KKT approach [16], [26] is used to determine the basis weights  $c$  of the observed trajectory, velocity, and acceleration, which are collectively denoted as  $\mathbf{Q}_{obs} = [\mathbf{q}_{obs}; \dot{\mathbf{q}}_{obs}; \ddot{\mathbf{q}}_{obs}]$ . Previous studies assume that the motion trajectory is segmented [21], [22] or that the motion consists of a single motion primitive or cost function [3], [24]. To the authors' knowledge, this paper is the first to remove the above assumptions. Instead, IOC is performed sequentially over sliding windows over the time series data. A change in the basis function weights is used to determine when the motion objective has changed, indicating a segment point. The approximate IOC method proposed in [16] is adapted to allow for changing basis weights by handling windows of arbitrary length and rejecting degenerate estimates.

This section describes two components of the optimal control process: direct optimal control (DOC), where  $c$  is known and  $\mathbf{Q}_{obs}$  is to be generated, and IOC, where  $\mathbf{Q}_{obs}$  is known, and  $c$  is to be estimated. The IOC estimates the basis weights  $\hat{c}$  based on  $\mathbf{Q}_{obs}$ , or parts of  $\mathbf{Q}_{obs}$ , while the DOC is used to generate simulation data and determine goodness-of-fit by comparing  $\mathbf{Q}_{obs}$  to its estimate  $\hat{\mathbf{q}}_{obs}$  as generated by  $\hat{c}$ .

### A. Trajectory Representation

The trajectories in this paper are represented as piecewise  $5^{th}$  order polynomials, where each individual polynomial is a spline of the form  $q_p = p_5 t^5 + p_4 t^4 + p_3 t^3 + p_2 t^2 + p_1 t + p_0$ . The spline is used to reduce the problem dimensionality by allowing modelling to occur on the spline control knots instead of the full trajectory, and to avoid bias in estimation [16]. It also allows for the trajectory derivatives to be estimated analytically.

Given the set of splining control knot locations  $t_{ck}$ , joint angles  $\mathbf{q}_{ck} = \mathbf{q}(t_{ck})$ , velocities  $\dot{\mathbf{q}}_{ck} = \dot{\mathbf{q}}(t_{ck})$ , and accelerations  $\ddot{\mathbf{q}}_{ck} = \ddot{\mathbf{q}}(t_{ck})$ , a polynomial is constructed between each pair of knots. The coefficients for the  $5^{th}$  order polynomial between control knot  $t_{ck,k}$  and  $t_{ck,k+1}$  are found by constructing a variation of the Vandermonde matrix  $\mathbf{V}$  [27]:

$$\mathbf{V} = \begin{bmatrix} t_k^5 & t_k^4 & t_k^3 & t_k^2 & t_k^1 & 1 \\ 5t_k^4 & 4t_k^3 & 3t_k^2 & 2t_k^1 & 1 & 0 \\ 20t_k^3 & 12t_k^2 & 6t_k^1 & 2 & 0 & 0 \\ t_{k+1}^5 & t_{k+1}^4 & t_{k+1}^3 & t_{k+1}^2 & t_{k+1}^1 & 1 \\ 5t_{k+1}^4 & 4t_{k+1}^3 & 3t_{k+1}^2 & 2t_{k+1}^1 & 1 & 0 \\ 20t_{k+1}^3 & 12t_{k+1}^2 & 6t_{k+1}^1 & 2 & 0 & 0 \end{bmatrix}$$

$$\mathbf{q}_c = [\dot{q}_k \quad \dot{q}_k \quad \ddot{q}_k \quad q_{k+1} \quad \dot{q}_{k+1} \quad \ddot{q}_{k+1}]$$

$$\mathbf{p} = \mathbf{V} \mathbf{q}_c^{-1} \quad (2)$$

where  $\mathbf{p}$  are the coefficients of the polynomial and the control knot subscript was removed for brevity (i.e.  $t_k = t_{ck,k}$ ). The number of control knots is a fixed value, and the control knots are evenly distributed in the window.

### B. Direct Optimal Control

Given  $c$  and  $t_{ck}$ , the goal of DOC is to generate the  $\mathbf{q}_{ck}$ ,  $\dot{\mathbf{q}}_{ck}$ , and  $\ddot{\mathbf{q}}_{ck}$  that minimize  $J(\mathbf{x})$ . These control knots, when optimized (denoted as  $\mathbf{q}_{ck}^*$ ), are used to generate a spline that approximates the optimal trajectory  $\mathbf{Q}_{obs} = \text{spline}(\mathbf{q}_{ck}^*, \dot{\mathbf{q}}_{ck}^*, \ddot{\mathbf{q}}_{ck}^*)$ . The general form of the constrained optimization problem is as follows:

$$\min_{\mathbf{x}} J(\mathbf{x}) \in h(\mathbf{x}) = 0, g(\mathbf{x}) \leq 0 \quad (3)$$

where  $h(\mathbf{x})$  are the equality constraints, and  $g(\mathbf{x})$  are the inequality constraints. The DOC problem is obtained by modifying Equation 3 into:

$$\min_{\mathbf{x}=\mathbf{q}_{ck}, \dot{\mathbf{q}}_{ck}, \ddot{\mathbf{q}}_{ck}} J(\mathbf{x}) = \sum_{i=0}^{n_{bf}} c_i J_{bf,i}(\mathbf{Q}_{obs}) \quad (4)$$

$$\in h(\mathbf{x}) = \begin{cases} \mathbf{q}(t_{const,q}) - \mathbf{q}_{const} = 0 \\ \dot{\mathbf{q}}(t_{const,dq}) - \dot{\mathbf{q}}_{const} = 0 \\ \ddot{\mathbf{q}}(t_{const,ddq}) - \ddot{\mathbf{q}}_{const} = 0 \end{cases}$$

where  $\mathbf{q}_{const}$ ,  $\dot{\mathbf{q}}_{const}$ , and  $\ddot{\mathbf{q}}_{const}$  denote the joint position, velocity, and acceleration constraints, respectively, and  $t_{const,q}$ ,  $t_{const,dq}$ ,  $t_{const,ddq}$  refer to their corresponding time points. These constraints form the equality constraints  $h(\mathbf{x})$  of the system. This paper does not include any inequality constraints  $g(\mathbf{x})$ , but potential inequality constraints can include joint and torque limits.

To solve the DOC problem, the trust region optimization method is used [28]. An initial trajectory is created by a  $5^{th}$  order polynomial, constrained for starting and ending  $\mathbf{q}$ ,  $\dot{\mathbf{q}}$ , and  $\ddot{\mathbf{q}}$ . The joint angles at  $t_{ck}$  are extracted from this trajectory and used to initialize  $\mathbf{q}(t_{ck})$ . At each optimization step,  $\mathbf{q}_{ck}$ ,  $\dot{\mathbf{q}}_{ck}$ , and  $\ddot{\mathbf{q}}_{ck}$  are used to create the spline, then all the features needed to calculate  $J_{bf}$  are determined. The features are normalized before  $J_{bf}$  calculations.

$$\begin{aligned}
\mathbf{A}_0 &= \begin{bmatrix} \nabla_{\mathbf{x}} J_{bf,1} & \nabla_{\mathbf{x}} J_{bf,2} & \cdots & \nabla_{\mathbf{x}} h_1 & \nabla_{\mathbf{x}} h_2 & \cdots \end{bmatrix} \\
&= \begin{bmatrix} \frac{\partial(J_{bf,1})}{\partial(q_{d=1,ck=1})} & \frac{\partial(J_{bf,2})}{\partial(q_{d=1,ck=1})} & \cdots & \frac{\partial(h_1)}{\partial(q_{d=1,ck=1})} & \frac{\partial(h_2)}{\partial(q_{d=1,ck=1})} & \cdots \\ \frac{\partial(J_{bf,1})}{\partial(q_{d=2,ck=1})} & \frac{\partial(J_{bf,2})}{\partial(q_{d=2,ck=1})} & \cdots & \frac{\partial(h_1)}{\partial(q_{d=2,ck=1})} & \frac{\partial(h_2)}{\partial(q_{d=2,ck=1})} & \cdots \\ \vdots & \vdots & \cdots & \vdots & \vdots & \cdots \\ \frac{\partial(J_{bf,1})}{\partial(q_{d=n_d,ck=n_{ck}})} & \frac{\partial(J_{bf,2})}{\partial(q_{d=n_d,ck=n_{ck}})} & \cdots & \frac{\partial(h_1)}{\partial(q_{d=n_d,ck=n_{ck}})} & \frac{\partial(h_2)}{\partial(q_{d=n_d,ck=n_{ck}})} & \cdots \\ \vdots & \vdots & \cdots & \vdots & \vdots & \cdots \\ \frac{\partial(J_{bf,1})}{\partial(\dot{q}_{d=n_d,ck=n_{ck}})} & \frac{\partial(J_{bf,2})}{\partial(\dot{q}_{d=n_d,ck=n_{ck}})} & \cdots & \frac{\partial(h_1)}{\partial(\dot{q}_{d=n_d,ck=n_{ck}})} & \frac{\partial(h_2)}{\partial(\dot{q}_{d=n_d,ck=n_{ck}})} & \cdots \\ \vdots & \vdots & \cdots & \vdots & \vdots & \cdots \\ \frac{\partial(J_{bf,1})}{\partial(\ddot{q}_{d=n_d,ck=n_{ck}})} & \frac{\partial(J_{bf,2})}{\partial(\ddot{q}_{d=n_d,ck=n_{ck}})} & \cdots & \frac{\partial(h_1)}{\partial(\ddot{q}_{d=n_d,ck=n_{ck}})} & \frac{\partial(h_2)}{\partial(\ddot{q}_{d=n_d,ck=n_{ck}})} & \cdots \end{bmatrix} \\
\mathbf{z}_0 &= [\hat{c}_1 \quad \hat{c}_2 \quad \cdots \quad \lambda_1 \quad \lambda_2 \quad \cdots]^T
\end{aligned}$$

Fig. 1. Formulation of the least squares problem for the IOC.  $\mathbf{A}_0$  denotes the gradient, differentiated against the  $k^{th}$  control knot point and  $d^{th}$  DOF, before the array is split and the pivot basis function is extracted.  $\mathbf{z}_0$  denotes the variables to recover.

### C. Inverse Optimal Control

In the IOC problem,  $\mathbf{q}_{ck}$  is known, and  $\mathbf{c}$  must be estimated. To achieve this, the IOC is formulated as an inverse KKT problem [29], [24], [16], [26]. By minimizing the residuals of the KKT equations, the system can achieve a near-optimal state. Given the problem formulation in Equation 4, the KKT Lagrangian  $L(\mathbf{x} = \mathbf{q}_{ck}, \dot{\mathbf{q}}_{ck}, \ddot{\mathbf{q}}_{ck})$  and its gradient  $\nabla_{\mathbf{x}} L(\mathbf{x})$  are defined as:

$$\begin{aligned}
L(\mathbf{x}) &= \sum_{i=0}^{n_{bf}} \hat{c}_i J_{bf,i}(\mathbf{Q}_{obs}) + \sum_{j=0}^{n_h} \lambda_j h_j(\mathbf{Q}_{obs}) \\
\nabla_{\mathbf{x}} L(\mathbf{x}) &= \sum_{i=0}^{n_{bf}} \hat{c}_i \nabla_{\mathbf{x}} J_{bf,i}(\mathbf{Q}_{obs}) + \sum_{j=0}^{n_h} \lambda_j \nabla_{\mathbf{x}} h_j(\mathbf{Q}_{obs})
\end{aligned}$$

where the partial differential of the gradient  $\nabla_{\mathbf{x}}$  is calculated with respect to the state variables  $\mathbf{q}_{ck}$ ,  $\dot{\mathbf{q}}_{ck}$ , and  $\ddot{\mathbf{q}}_{ck}$ ,  $\lambda$  are the Lagrangian multipliers on  $h(\mathbf{x})$ , and  $\mathbf{Q}_{obs}$  is constructed from the spline representation of the trajectory. The condition that must be met to ensure optimality is:

$$\nabla_{\mathbf{x}} L(\mathbf{Q}_{obs}) = 0 \quad (5)$$

If it is assumed that the system is not strictly optimal, but rather only approximately optimal [29], then Equation 6 is minimized but is not strictly zero:

$$\begin{aligned}
\min_{\hat{\mathbf{c}}, \lambda} \nabla_{\mathbf{x}} L(\mathbf{Q}_{obs}) \\
\in \hat{\mathbf{c}} \geq 0
\end{aligned} \quad (6)$$

Since the KKT equations are linear with respect to the unknown variables  $\hat{\mathbf{c}}$  and  $\lambda$ , Equation 6 can be written as a least square problem in the form of  $\mathbf{A}\mathbf{z}$ , as shown in Figure 1, and solved computationally efficiently. To solve this constrained linear least squares problem, the active set method is used [30]. The gradient is calculated numerically.

In order to prevent trivial solutions, one of the values of  $\hat{\mathbf{c}}$  must be set to a non-zero value. This term, denoted as

the *pivot*, may be selected with some prior knowledge of the nature of the cost functions [31]. In this paper, no prior knowledge is assumed, so all basis functions will be used as the pivot, and the best fit will be selected by selecting the entry with the smallest KKT error residual. To construct the pivot  $\mathbf{b}_i$ , the  $i^{th}$  column of  $\mathbf{A}_0$ ,  $c_i$  is constrained to be 1.

The IOC process is applied on a sliding window of arbitrary length over the  $\mathbf{Q}_{obs}$  to recover the  $\hat{\mathbf{c}}$  of the trajectory over that window. Depending on the size and location of the window in the time series data stream, it may not be possible to recover the weights, leading to a degenerate solution. In these cases, the error residual from Equation 6 is very high, and typically corresponds to a negative  $\hat{\mathbf{c}}$  if the  $\mathbf{c} \geq 0$  optimization constraint in Equation 6 is relaxed. To detect these degenerate solutions, the residual norm  $\|\mathbf{A}_i \mathbf{z}_i + \mathbf{b}_i\|_2^2$  can be checked as an indicator of the quality of the  $\hat{\mathbf{c}}$  estimates. Once the pivot has been selected, the trajectory  $\hat{\mathbf{q}}_{obs}$  corresponding to  $\hat{\mathbf{c}}$  can be generated via DOC.

In simulation, degenerate cases can also be detected by comparing the estimated  $\hat{\mathbf{c}}$  against the ground truth  $\mathbf{c}$  used to generate the test trajectory. For human data, there is no way to determine the ground truth  $\mathbf{c}$  to verify  $\hat{\mathbf{c}}$ . Therefore, the thresholds for detecting degenerate cases were estimated from simulations and are reported in Table I. The basis functions used to determine the thresholds are  $J_{ddq}$ ,  $J_{ddx}$ , and  $J_{\tau}$ . Windows that are below the residual norm threshold are considered sufficiently optimal.

TABLE I  
RESIDUAL NORM THRESHOLD VALUES DETERMINED BY SIMULATION  
FOR THE SQUAT MOTION.

Window length [s]	0.6	0.8	1.0	1.2	1.4	1.6
Threshold [ $\times 10^{-3}$ ]	5.0	6.4	4.5	3.5	3.0	2.5

The optimal windows are then aggregated into a single trajectory or value, denoted as the *blended metric*, which is obtained by extracting all the windows that contain  $t$  and

averaging the metric over all of the extracted windows. For example, the blended  $\bar{c}_t$  at time  $t$  is calculated by selecting all the windows  $\omega$  that overlap with  $t$ , and calculating the average  $\hat{c}$  over the  $n_w$  selected windows:

$$\bar{c}_t = \sum \frac{\hat{c}}{n_w} \quad \forall t \in \omega$$

The blended  $\bar{q}_{obs}$  at time  $t$  is calculated similarly, by selecting all the windows that overlap with  $t$ , and averaging all the  $\hat{q}_{obs}$  values of the selected windows. The blended RMSE is then calculated between input trajectory  $Q_{obs}$  and the estimated blended  $\bar{q}_{obs}$ .

### III. SOURCES OF DATA

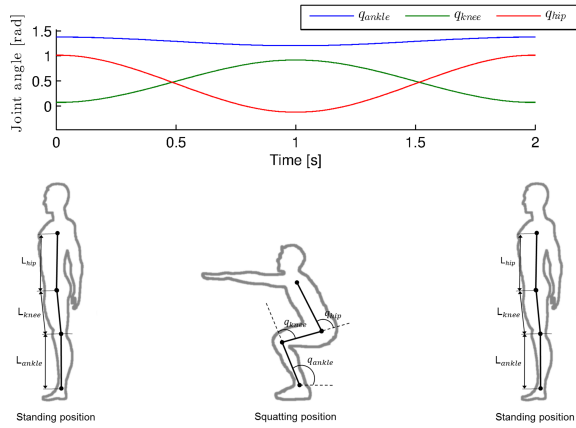


Fig. 2. Generation of the simulation squat DOC. The first and third set of  $h(\mathbf{x})$  constraints denote the standing position, where the  $\mathbf{q}$  are set to simulate a standing person, and the second set of  $h(\mathbf{x})$  constraints denote the squatting position. All  $h(\mathbf{x})$  constraints corresponding to the  $\dot{\mathbf{q}}$  and  $\ddot{\mathbf{q}}$  are zero, denoting a stationary person at the key poses.

The proposed approach was tested in two sets of experiments. The first set of experiments simulated squats and hip extension motions, while the second set examined human squat data. Squats and hip extensions were chosen for this experiment as they are common, well-known full-body exercises used in both athletics and rehabilitation [32].

#### A. Simulation Data

In the first experiment, DOC was used to generate a set of  $Q_{obs}$  with a known set of  $c$  values, which can be used as the ground truth for algorithm validation. Multiple repetitions of a squat or hip extension task were simulated by minimizing  $J_{ddq}$ ,  $J_{ddx}$ , and  $J_{\tau au}$  (Table I), or a weighted sum of all three criteria. Each repetition had 9  $h(\mathbf{x})$  constraints, corresponding to the position, velocity, and acceleration constraints for 3 key poses during the task: standing, squatting or hip extension, then standing again, placed at the start, middle, and end of the DOC trajectory (Figure 2). Each repetition had a duration of 2 s.  $Q_{obs}$  was modelled as 3 degrees of freedom (DOFs) system, corresponding to the ankle  $q_{ankle}$ , knee  $q_{knee}$ , and hip  $q_{hip}$ .

TABLE II  
BASIS FUNCTIONS USED [21], SUMMED OVER ALL  $n_d$  DOFS AND  $T$  TIME.  $M$  DENOTES THE INERTIAL MATRIX.

Angular acceleration (ddq)	$J_{ddq} = \sum_d \sum_t \ddot{q}_{d,t}^2$
Angular jerk (dddq)	$J_{dddq} = \sum_d \sum_t \dddot{q}_{d,t}^2$
Cartesian acceleration (ddx)	$J_{ddx} = \sum_t \ddot{x}_{n_d,t}^2$
Cartesian jerk (dddx)	$J_{dddx} = \sum_t \dddot{x}_{n_d,t}^2$
Torque (tau)	$J_{\tau au} = \sum_d \sum_t \tau_{d,t}^2$
Torque change (dtau)	$J_{d\tau au} = \sum_d \sum_t \dot{\tau}_{d,t}^2$
Torque effort (ddtau)	$J_{dd\tau au} = \sum_d \sum_t \ddot{\tau}_{d,t}^2$
Kinetic energy (en)	$J_{en} = \sum_d \sum_t \dot{q}_{d,t} M(\mathbf{q}) \dot{q}_{d,t}$
Power	$J_{power} = \sum_d \sum_t (\dot{q}_{d,t} \tau_{d,t})^2$

#### B. Human Data

In the second experiment, segmentation was performed on an experimental dataset. An 8-subject dataset [33] of healthy participants with an average age of  $30 \pm 5$  years old performing an average of 10 squats each were collected using a VICON motion capture system. A 10 marker model was used, providing joint Cartesian position data. Joint angles were calculated from the cross products between markers, using a 3 DOF planar kinematic model, corresponding to  $q_{ankle}$ ,  $q_{knee}$ , and  $q_{hip}$ .

### IV. EXPERIMENTAL RESULTS

#### A. IOC Reconstruction

For IOC reconstruction,  $n_{ck}$  was set to 5 points every 1 s, evenly distributed over  $Q_{obs}$ . A sliding window, incrementing by 0.2 s, was passed over the trajectory.  $h(\mathbf{x})$  constraints were set so that the joint position, velocity, and acceleration constraints were placed at the start, middle, and end of the IOC window. The IOC pivot that resulted in the smallest residual was selected as the most suitable pivot. Any window that led to a reconstruction that has a residual norm that exceeds the tuned threshold in Table I was rejected.

The basis functions considered in this paper, motivated by [21], can be found in Table II. All features were calculated from the joint angle measurements. Angular acceleration  $\ddot{\mathbf{q}}$  and jerk  $\dddot{\mathbf{q}}$  values were calculated from the derivatives of the joint angle spline. The Cartesian acceleration  $\ddot{\mathbf{x}}$  values were calculated via forward kinematics, while the Cartesian jerk  $\dddot{\mathbf{x}}$  values were calculated from numerical differentiation of the Cartesian acceleration. Torque  $\tau$  values were calculated using anthropometric table [34] data for the dynamic

TABLE III

THE EFFECTS OF VARYING WINDOW LENGTH ON THE DATAPPOINTS THAT ARE BELOW THE RESIDUAL NORM THRESHOLD AND THE MEAN BLENDED RMSE. BOLD DENOTES THE WINDOW SIZE WITH THE MOST POINTS PASSING THE RESIDUAL NORM THRESHOLD.

Length [s]	Residual Pass [%]	Blended RMSE [ $\times 10^{-3}$ rad]
<b>0.6</b>	<b>78.68</b>	<b>0.0</b>
0.8	66.9	0.0
1.0	50.8	0.0
1.2	40.6	0.0
1.4	32.9	0.0
1.6	25.1	0.0

parameters and inverse dynamics through Symoro [35]:

$$\tau = M(\mathbf{q})\ddot{\mathbf{q}} + C(\mathbf{q}, \dot{\mathbf{q}}) + G(\mathbf{q})$$

where  $M(\mathbf{q})$  is the inertia matrix,  $C(\mathbf{q}, \dot{\mathbf{q}})$  is the Coriolis matrix, and  $G(\mathbf{q})$  is the gravity vector. Torque change  $\dot{\tau}$  and effort  $\dot{\tau}$  values were obtained from numerical differentiation. All calculations were done in MATLAB 8.0.

### B. Simulation

Experiments with the simulation data show that degenerate situations can occur in two different cases. The first case is if the basis functions hypothesized during IOC do not correspond to the cost function used to generate the motion. This leads to an  $\mathbf{A}_0$  matrix that does not provide the correct basis functions that can sufficiently minimize Equation 6 and leads to a high residual norm value. These cases can be rejected by the residual norm threshold test if properly tuned. See Figure 3 for examples of the simulation reconstruction.

The second case is if the windowed part of the trajectory does not provide sufficient information for the IOC model. This could happen if the window is insufficiently long, or if there are the same or more  $h(\mathbf{x})$  constraints than knot points (i.e.  $n_h \geq n_{ck}$ ) in the IOC window. In this case, the residual norm test will be inaccurate, especially if there are enough  $h(\mathbf{x})$  constraints to satisfy the least squares without the basis function columns in the  $\mathbf{A}_0$  matrix, which will result in a low residual norm value but a degenerate case. This can be avoided by ensuring that all IOC windows have more control knots than  $h(\mathbf{x})$  constraints.

### C. Human Data

Table III shows the impact of varying window size, indicating that a window width of 0.6 s provided the highest percentage of windows that are below the residual norm threshold. Testing showed that window length smaller than 0.6 s fell into the second case described in Section IV-B and were not considered. Given that the average squat motion is approximately 2 s to 2.5 s long, a window of 0.6 s represents about a quarter of the motion of interest. The remaining 21.3% that was rejected by the residual norm threshold may be a result of poor cost function modelling, i.e., that the true cost functions required to model these specific parts of the trajectory are not included into the model. The larger the window, the worse the performance, implying that good

recovery is not possible when the cost function is in the process of changing or that more complex cost functions may be required to capture longer sequences of the observed data.

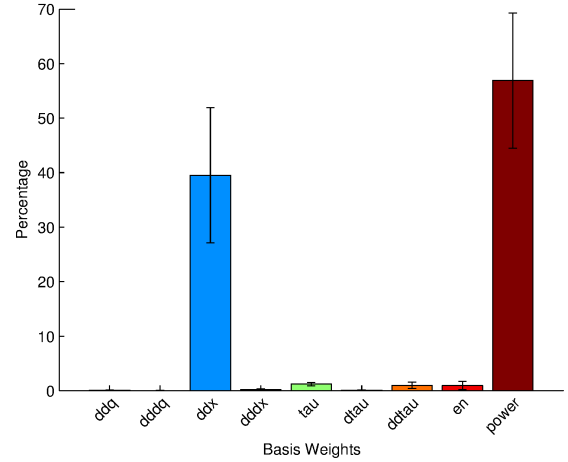
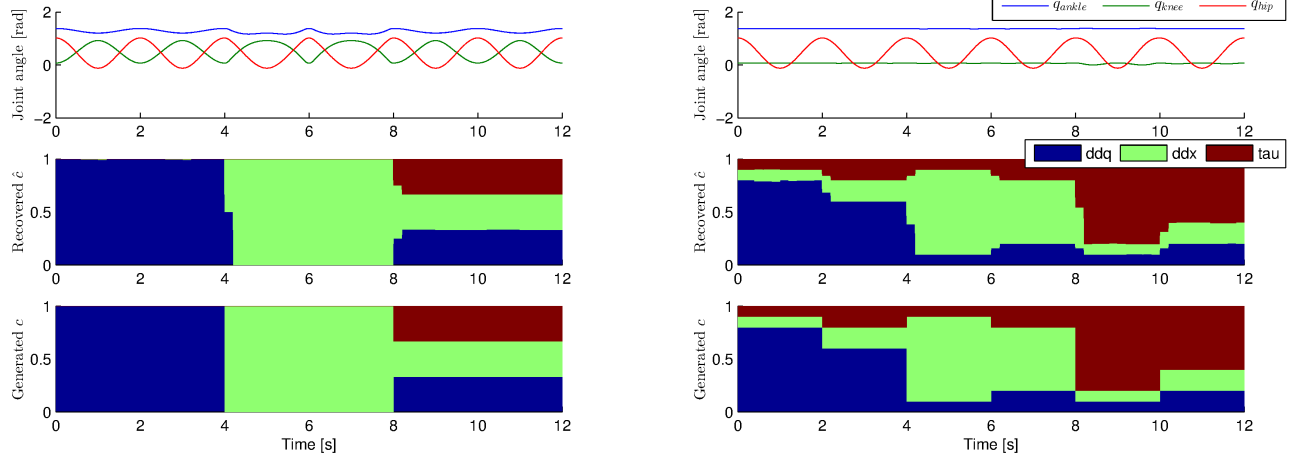


Fig. 4. Percentage of  $\hat{\mathbf{c}}$  over 8 subjects. This plot was generated by calculating the mean  $\hat{\mathbf{c}}$  over the full trajectory of each subject, resulting in 8 sets of  $\hat{\mathbf{c}}$ . The mean and standard deviation in this graph shows the mean and variation between participants. The IOC recovery suggests that  $c_{power}$  and  $c_{ddx}$  contribute a significant amount of the basis weights for the squat motion.

Figure 5 shows the weight recovery of two different subjects, where Figure 5b has a high number of residual norm test passes, while Figure 5c has a low number of residual norm passes. These two figures show that the proposed method clearly delineates between the squat motion and its high  $c_{ddx}$  weight (blue), and the resting periods and its high  $c_{power}$  weight (red), and can be used for segmentation. Figure 4 shows that this distribution of the basis function weights is common for all participants examined. While the percentage allocated to minimizing  $J_{power}$  and  $J_{ddx}$  may change, as indicated from the large standard deviations on these two basis weights, they are much higher than all other basis functions, indicating that they are more important in the squatting movement strategy. This finding is similar to previous findings, where acceleration [3] and power [21] have been found to be important basis functions.

Figure 5 also shows that the trajectory in motion has a higher tendency to be rejected due to higher residuals, as denoted by the indicators at the bottom of the joint angle plots, where red dots denote no windows passed the residual test at that timestep, yellow dots denote that only 1 window passed the residual test, while green dots denote that more than 1 window passed the residual test. This is also reflected in the gaps in the  $\hat{\mathbf{c}}$  plot, as no basis weights are available for timesteps that did not have any successful estimate. This suggests that, at least for the motion in Figure 5c, either that the current set of basis functions may not be sufficient to model the motion at its turning points, or that the cost function is changing too rapidly and may benefit from a smaller window. Table IV shows that raising the residual threshold allows more windows to pass.



(a) Squat data with the residual norm threshold at  $5 \times 10^{-3}$ . The simulated cost vectors are  $[1; 0; 0]$ ,  $[0; 1; 0]$ , and  $[1; 1; 1]$ . (b) Hip extension data with the residual norm threshold at  $1 \times 10^{-3}$ . The simulated cost vectors are  $[0.8; 0.1; 0.1]$ ,  $[0.6; 0.2; 0.2]$ ,  $[0.1 \ 0.8 \ 0.1]$ ,  $[0.2 \ 0.6 \ 0.2]$ ,  $[0.1 \ 0.1 \ 0.8]$ , and  $[0.2 \ 0.2 \ 0.6]$ .

Fig. 3. Simulation data, illustrating  $Q_{obs}$  (top), the recovered blended  $\hat{c}$  (middle), and the original  $c$  (bottom). The data was created using three basis functions,  $J_{ddx}$  (blue),  $J_{ddq}$  (green) and  $J_{\tau}$  (red), and varying the cost weights. The jagged components in the  $\hat{c}$  plot are caused by window averaging when a given window overlaps two different basis functions.

TABLE IV

THE EFFECTS OF RESIDUAL THRESHOLD (THRES,  $[\times 10^{-3}]$ ) ON SQUAT DATA ON RESIDUAL PASS RATE, RMSE, AND SEGMENTATION BALANCED ACCURACY OVER THE 8 SUBJECTS. BLENDED RMSE IS THE RESULT OF THE BLENDED  $\bar{q}_{obs}$  OF ALL THE IOC WINDOWS THAT PASSED THE THRESHOLD COMPARED AGAINST  $Q_{obs}$ , WHILE WINDOWED RMSE IS THE RESULT OF EACH IOC WINDOW AGAINST ITS WINDOWED  $Q_{obs}$ .

Subject	Residual Pass [%]			Blended RMSE $[\times 10^{-3}$ rad]			Windowed RMSE $[\times 10^{-3}$ rad]			Segmentation [%]			
	Thres	5	10	50	5	10	50	5	10	50	5	10	50
1		91.8	98.2	100.0	3.1	3.2	3.3	$1.9 \pm 3.9$	$2.1 \pm 4.1$	$2.3 \pm 4.2$	90.9	90.5	90.5
2		68.8	73.5	84.9	3.2	4.0	5.2	$1.4 \pm 2.7$	$1.8 \pm 4.0$	$2.7 \pm 5.5$	81.4	83.6	83.5
3		89.5	96.3	100.0	3.5	3.9	4.1	$2.5 \pm 3.9$	$2.9 \pm 4.6$	$3.1 \pm 4.8$	90.6	90.9	90.9
4		91.5	98.8	100.0	4.3	5.0	6.2	$2.9 \pm 5.1$	$3.4 \pm 5.9$	$4.1 \pm 7.4$	85.7	85.8	85.3
5		54.3	63.0	86.5	4.8	5.0	7.8	$3.6 \pm 4.9$	$3.8 \pm 5.1$	$5.8 \pm 8.1$	81.9	82.7	83.7
6		91.7	97.3	100.0	3.8	4.8	4.8	$2.4 \pm 4.4$	$2.8 \pm 5.4$	$2.9 \pm 5.4$	84.6	83.6	83.4
7		81.0	91.5	98.4	4.2	4.4	5.5	$2.6 \pm 4.2$	$3.3 \pm 5.0$	$4.2 \pm 6.1$	86.1	87.7	87.8
8		56.2	66.7	95.4	3.4	5.9	9.6	$2.0 \pm 3.4$	$2.9 \pm 7.2$	$5.0 \pm 12.1$	88.4	87.9	89.2

Increasing the threshold had the effect of increasing both the blended and windowed RMSE, as more windows that are less optimally solved are now being included.

Table IV also shows the accuracy of a threshold based segmentation approach. The trajectory is separated into two classes, where periods of motion are considered as true positives (TP), periods of rest are considered as true negatives (TN), false motion as false positives (FP), and false rest is false negative (FN). The values in Table IV were obtained by thresholding the most influential basis weight,  $\hat{c}_{power}$ , and selecting the threshold ( $\hat{c}_{power} = 0.55$ ) that resulted in the best accuracy rating. The accuracy metric utilized is the balanced accuracy ( $0.5 \cdot (\frac{TP}{TP+FN} + \frac{TN}{TN+FP})$ ).

## V. CONCLUSION

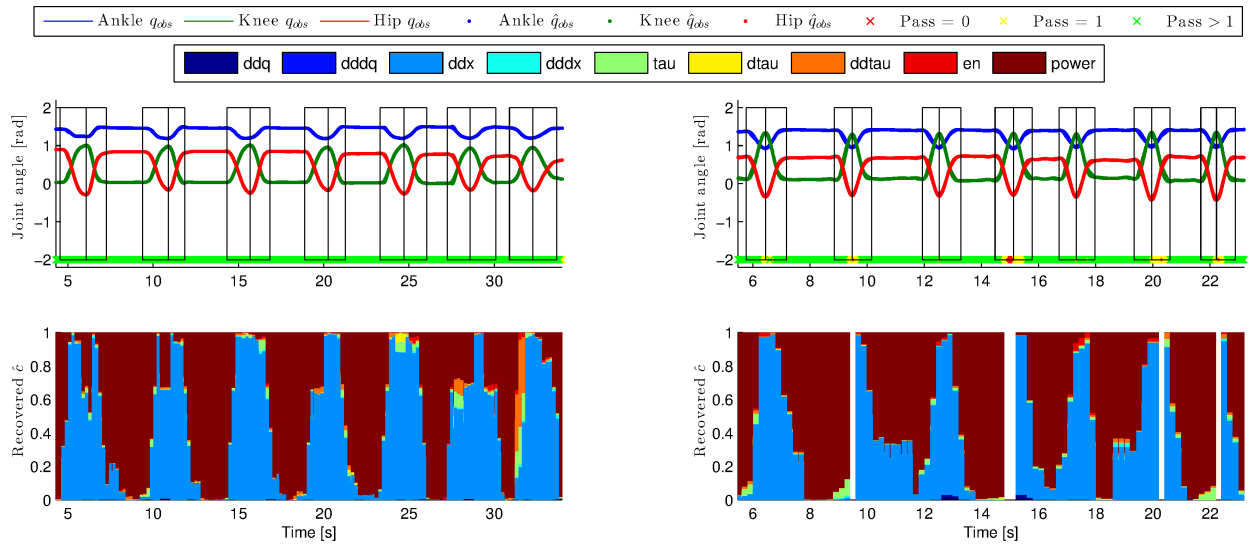
This paper proposes a method for human motion segmentation based on inverse optimal control. The approach accepts arbitrary lengths of trajectories and estimates the underlying basis function weights for successive windows of that trajectory using inverse optimal control. A method to

reject low-quality weight estimates by examining the residual norm is proposed, and the algorithm is demonstrated in both simulation and with real data. The basis weights of a set of squat tasks suggests that humans optimize for power and Cartesian acceleration during rest and movement, respectively, and that this choice of cost functions is consistent across the 8 healthy subjects in the dataset. It was also shown that a threshold-based segmentation method on the power basis weight achieved 84% in balanced accuracy.

For future work, online recovery of weights for online segmentation will be explored. In imitation learning or rehabilitation applications, immediate user feedback is desirable so that the users can adjust erroneous movements quickly; this requires fast and robust segmentation algorithms. Additional basis functions and datasets will also be explored.

## REFERENCES

- [1] R. M. Alexander, "The gaits of bipedal and quadrupedal animals," *Int J Robot Res*, vol. 3, pp. 49–59, 1984.
- [2] T. Flash and N. Hogan, "The coordination of arm movements: an experimentally confirmed mathematical model," *J Neurosci*, vol. 5, pp. 1688–1703, 1985.



(a) Subject 1, with 91% of the windows passing the residual threshold.

(b) Subject 5, with 54% of the windows passing the residual threshold.

Fig. 5.  $Q_{obs}$  (top, thin) and  $\hat{Q}_{obs}$  (top, thick) trajectory with pass markers (top, light green) and the normalized  $\hat{\epsilon}$  (bottom) of two different subjects with the threshold at  $5 \times 10^{-3}$ . Timepoints that do not have any windows below the residual threshold are not filled in, leaving a gap in the  $\hat{\epsilon}$  and the  $\hat{Q}_{obs}$ . The markers at the bottom of the trajectory plot indicate the number of windows used to generate that timestep, and is delineated to be 0 (red), 1 (yellow), or greater than 1 (green).

- [3] K. Mombaur *et al.*, "From human to humanoid locomotion an inverse optimal control approach," *Auton Robot*, vol. 28, pp. 369–383, 2010.
- [4] E. Todorov, "Optimality principles in sensorimotor control," *Nat Neurosci*, vol. 7, pp. 907–915, 2004.
- [5] J. F.-S. Lin *et al.*, "Movement primitive segmentation for human motion modeling: A framework for analysis," *IEEE Trans Human-Mach Syst*, vol. 46, pp. 325–339, 2016.
- [6] S. Calinon *et al.*, "Learning and reproduction of gestures by imitation," *IEEE Robot Autom Mag*, vol. 17, pp. 44–54, 2010.
- [7] C. Breazeal *et al.*, "Effects of nonverbal communication on efficiency and robustness in human-robot teamwork," in *IEEE RSJ Conf Intellig Robot Syst*, 2005, pp. 708–713.
- [8] A. W. K. Lam *et al.*, "Automated rehabilitation system: Movement measurement and feedback for patients and physiotherapists in the rehabilitation clinic," *Hum Comput Int*, vol. 31, pp. 294–334, 2016.
- [9] T. B. Moeslund *et al.*, "A survey of advances in vision-based human motion capture and analysis," *Comput Vis Image Und*, vol. 104, pp. 90–126, 2006.
- [10] D. Kulić *et al.*, "Online segmentation and clustering from continuous observation of whole body motions," *IEEE Trans Robot*, vol. 25, pp. 1158–1166, 2009.
- [11] J. F.-S. Lin and D. Kulić, "On-line segmentation of human motion for automated rehabilitation exercise analysis," *IEEE Trans Neural Syst Rehabil Eng*, vol. 22, pp. 168–180, 2014.
- [12] F. Lv and R. Nevatia, "Recognition and segmentation of 3-D human action using HMM and multi-class AdaBoost," in *Comput Vis Image Und*, 2006, pp. 359–372.
- [13] F. Bashir *et al.*, "HMM-based motion recognition system using segmented PCA," in *IEEE Conf Image Proc*, 2005, pp. 1288–1291.
- [14] T. Aoki *et al.*, "Segmentation of human body movement using inertial measurement unit," in *IEEE Conf Syst Man Cybern*, 2013, pp. 1181–1186.
- [15] F. Chamroukhi *et al.*, "Joint segmentation of multivariate time series with hidden process regression for human activity recognition," *Neurocomputing*, vol. 120, pp. 633–644, 2013.
- [16] A. M. Panchea and N. Ramdani, "Towards solving inverse optimal control in a bounded-error framework," in *Am Contr Conf*, 2015, pp. 4910–4915.
- [17] D. Clever *et al.*, "Inverse optimal control based identification of optimality criteria in whole-body human walking on level ground," in *IEEE EMBS Conf Biomed Robot Biomech*, 2016, pp. 1192–1199.
- [18] A. V. Papadopoulos *et al.*, "Generation of human walking paths," *Auton Robot*, vol. 40, pp. 59–75, 2016.
- [19] D. Clever and K. Mombaur, "A new template model for optimization studies of human walking on different terrains," in *IEEE RAS Conf Humanoid Robot*, 2014, pp. 500–505.
- [20] S. Albrecht *et al.*, "Imitating human reaching motions using physically inspired optimization principles," in *IEEE RAS Conf Humanoid Robot*, 2011, pp. 602–607.
- [21] B. Berret *et al.*, "Evidence for composite cost functions in arm movement planning: An inverse optimal control approach," *PLoS Comput Biol*, vol. 7, pp. 1–18, 2011.
- [22] N. Sylla *et al.*, "Human arm optimal motion analysis in industrial screwing task," in *IEEE EMBS Conf Biomed Robot Biomech*, 2014, pp. 964–969.
- [23] S. Boyd and L. Vandenberghe, *Convex Optimization*. Cambridge Univ, 2004.
- [24] A.-S. Puydupin-Jamin *et al.*, "A convex approach to inverse optimal control and its application to modeling human locomotion," in *IEEE Conf Robot Autom*, 2012, pp. 531–536.
- [25] N. Aghasadeghi and T. Bretl, "Inverse optimal control for differentially flat systems with application to locomotion modeling," in *IEEE Conf Robot Autom*, 2014, pp. 6018–6025.
- [26] P. Englert and M. Toussaint, "Inverse KKT – Learning Cost Functions of Manipulation Tasks from Demonstrations," in *Symp Robot Res*, 2015, pp. 1–16.
- [27] M. W. Spong *et al.*, *Robot Modeling and Control*. John Wiley, 2006.
- [28] R. H. Byrd *et al.*, "A trust region method based on interior point techniques for nonlinear programming," *Math Prog*, vol. 89, pp. 149–185, 2000.
- [29] A. Keshavarz *et al.*, "Imputing a convex objective function," in *IEEE Symp Intelligent Control*, 2011, pp. 613–619.
- [30] P. E. Gill *et al.*, *Practical Optimization*. Academic Press, 1981.
- [31] A. M. Panchea, "Inverse optimal control for redundant systems of biological motion," Ph.D. dissertation, Universit es d'Orleans, 2015.
- [32] C. Kisner and L. A. Colby, *Therapeutic Exercise: Foundations and Techniques*. Davis, 2007.
- [33] V. Bonnet *et al.*, "A least-squares identification algorithm for estimating squat exercise mechanics using a single inertial measurement unit," *J Biomech*, vol. 45, pp. 1472–1477, 2012.
- [34] R. Dumas *et al.*, "Adjustments to McConville *et al.* and Young *et al.* body segment inertial parameters," *J Biomech*, vol. 40, pp. 543–553, 2007.
- [35] W. Khalil and D. Creusot, "Symoro+: A system for the symbolic modelling of robots," *Robotica*, vol. 15, pp. 153–161, 1997.